Pergamon

Int. J. Heat Mass Transfer. Vol. 38, No. 18, pp. 3319–3328, 1995

0017–9310/95 $9.50 + 0.00

0017–9310(95)00080–1

Three-dimensional driven-cavity flows with a vertical temperature gradient

REIMA IWATSU

Obayashi Corporation Technical Research Institute, 4-640 Simokiyoto, Kiyose-Shi, Tokyo 204, Japan

and

JAE MIN HYUN

Korea Advanced Institute of Science and Technology, 373-1 Kusong-Ku, Taejon 305-701, Korea

(*Received* 23 *August* 1994 *and in final form* 2 *March* 1995)

Abstract—Numerical studies of three-dimensional flows in a cubical container with a stable vertical temperature stratification are carried out. Flows are driven by the top lid, which slides in its own plane at a constant speed. The top wall is maintained at a higher temperature than the bottom wall. The end walls and the side walls are thermally insulated. Numerical solutions are obtained over a wide range of physical parameters, i.e. $10^2 \leqslant Re \leqslant 2 \times 10^3$, $0 \leqslant Ri \leqslant 10.0$ and $Pr = 0.71$, where the mixed-convection parameter $Ri \equiv Gr \cdot Re^{-2}$. Systematical comparison of the three-dimensional numerical solutions with the previously reported two-dimensional results illuminates the impact of thermal stratification on the three-dimensional flow characteristics. When $Ri \ll O(1)$, the effect of the vertical temperature gradient is minor, and the flow structures are similar to those of the non-stratified fluid flows in a conventional lid-driven cavity flow. Fluids in the primary vortex are well mixed, and the temperature is fairly uniform in the main circulating region. When $Ri \geqslant O(1)$, the stable temperature distribution tends to suppress the vertical fluid motion. Much of the fluid motion takes place in the vicinity of the top sliding lid and the bulk of the cavity region is nearly stagnant. When $Ri \gg O(1)$, the fluid motion exhibits vertically layered vortex structures. The Nusselt number is computed at the top and bottom wall, and this also illustrates the varying flow characteristics as Ri encompasses a broad range. Extensive numerical flow visualizations are conducted. Plots demonstrating the primary flows in the $(x$–$y)$ plane and the secondary flows in the $(y$–$z)$ plane are presented. These display the influences of Re and Ri on the basic character of the flow and the three-dimensional effects.

1. INTRODUCTION

Flows of a viscous fluid in a closed enclosure, driven by a boundary wall sliding at constant speed U_0 in its own plane, constitute a classical model problem. In its simplest form, the two-dimensional problem in a square cavity of height h is often referred to as the standard driven-cavity flows. The flow is characterized by the Reynolds number, $Re \equiv U_0 h/\nu$, where ν denotes kinematic viscosity of the fluid. This problem offers an attractive testing ground to validate numerical solution algorithms [1]. The boundary conditions are straightforward, and various numerical solutions are cross-checked to assess the capabilities of newly-developed numerical methodologies. On the experimental front, flow visualization and measurement techniques are introduced and put to work on this benchmark problem formulation [2–9].

The majority of past numerical efforts on driven-cavity flows have been confined to two-dimensional configurations. Due to the recent innovations in computing technologies, several serious endeavors have been reported in the literature to tackle realistic three-dimensional cavity flows. Among others, Freitas *et al.* [10, 11] computed flow in a rectangular cavity of depth-to-spanwise aspect ratio 3.0 at $Re = 3200$. The existence of meridional vortices was documented and considerable flow unsteadiness was noted. Prasad *et al.* [6], in a calculation similar to that of Freitas *et al.*, varied the spanwise aspect ratio between 0.25 and 1.0. The findings were shown to be qualitatively consistent with the experimental observations by Koseff and Street [2–4]. Ku *et al.* [12] calculated flows in a cubic cavity at $Re = 1000$ and 100,400. Perng and Street [13] computed flow at a higher Re, i.e. $Re = 3200$. A systematic computational exercise was performed by Iwatsu *et al.* [14, 15] for a cubic cavity for $100 \leqslant Re \leqslant 4000$. These numerical programs illustrated the prominent flow characteristics as Re encompassed a wide range, and the emergence of three-dimensional Taylor–Görtler-like vortices was discernible. The results of three-dimensional flow computations were shown to be in broad qualitative agreement with the published experimental data. These positive comparisons give credence to the accuracy and robustness of numerical approaches in dealing with three-dimensional driven-cavity flows.

NOMENCLATURE

g	gravity acceleration	ΔT	temperature difference, $T_T - T_B (\Delta T > 0)$
Gr	Grashof number, $\alpha g \Delta T h^3/\nu^2$	U_0	top wall velocity
h	cavity height	$\mathbf{V}$	nondimensional velocity vector, (u, v, w)
$\bar{N}u$	average Nusselt number [equation (4)]	x, y, z	coordinate (see Fig. 1).
p	nondimensional pressure		
Pr	Prandtl number, ν/κ	Greek symbols	
Re	Reynolds number, $U_0 h/\nu$	α	coefficient of thermometric expansion
Ri	Richardson number, $Gr \cdot Re^{-2}$	κ	thermal conductivity
t	nondimensional time	ν	kinematic viscosity
T	nondimensional temperature, $(T_{dim} - T_B)/\Delta T$	ρ	density.
T_B	bottom wall temperature		
T_T	top wall temperature		

We shall now consider driven-cavity flows when a vertical temperature difference is applied at the horizontal surface walls of the container. This implies that an additional element, buoyancy, is brought into the overall dynamics. The impact of buoyancy on general flow patterns in a driven-cavity was studied by numerical [16–18] and experimental investigations [19]. In particular, the work of Mohamad and Vistanka [18] considered the flows in a shallow two-dimensional rectangular cavity when a gravitationally destabilizing vertical temperature difference, i.e. bottom-heated and top-cooled, was enforced. The numerical studies of Iwatsu *et al.* [16, 17] addressed the issues of flow and heat transport in a two-dimensional cavity when a stabilizing vertical temperature difference, i.e. bottom-cooled and top-heated, was applied. The purpose was to inquire as to the possibility of heat transfer augmentation by enhancing convective activities in an otherwise conduction-controlled enclosed container. The above studies clearly illustrated complex interplays between mechanically caused convection and gravitational buoyancy effects. Iwatsu *et al.* [16, 17] documented the changes in global heat transports as the mixed-convection parameter $Ri[\equiv Gr \cdot \mathrm{Re}^{-2}]$, where Gr is the system Grashof number, covered a broad range.

In the present paper, efforts are undertaken to extend the previous work of Iwatsu *et al.* [16, 17] to a three-dimensional cavity. The objective is to move the above analyses closer to realism. The mission is to seek full numerical solutions to three-dimensional driven-cavity flow and heat transfer characteristics over ranges of principal nondimensional parameters. As stressed earlier, since the externally-applied temperature difference is gravitationally stable, the vertical heat transfer would be entirely conductive in the absence of the top lid motion. By forcing the lid to slide, mechanically driven convection is induced, and the associated heat transports are enhanced. In realistic applications, however, three-dimensional constraints have to be taken into consideration, and the present paper aims to disclose three-dimensional features in a cubic cavity. Of particular interest will be the depiction of three-dimensionalities in the relevant parameter spaces. These will also help identify the limitations of two-dimensional computational results. A series of numerically-constructed plots, exhibiting the primary flows on the $(x$–$y)$ plane and the meridional flows on the $(y$–$z)$ plane, will be presented. These will point to the influences of mechanically- and thermally-driven convections on the main and transverse flows. Perspective views are made to portray the three-dimensional temperature fields and heat transfer at the walls.

2. NUMERICAL MODEL

Consider a viscous, incompressible fluid of density ρ and thermal diffusibity κ, filled in a cubic cavity, sketched in Fig. 1. The top lid, $y = h$, executes a steady sliding motion in its own plane at constant velocity U_0, and the other boundary walls are at rest. The top and bottom lids are thermal conductors with prescribed temperatures, T_T and T_B, with $\Delta T \equiv T_T - T_B > 0$, respectively. The other boundary surfaces are thermally insulated. The task is to describe the fluid flow and heat transfer in the cavity.

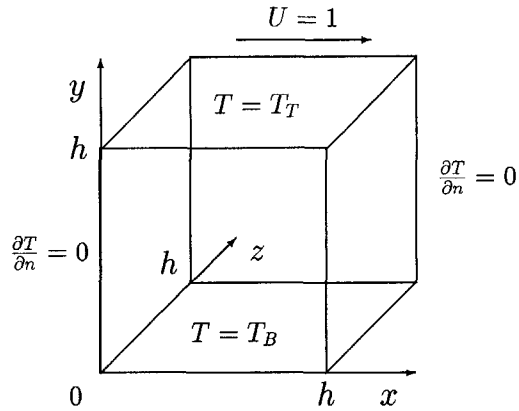

Fig. 1. Boundary condition and flow configuration.

The governing, three-dimensional Navier–Stokes equations are written, in nondimensionalized form, as:

$$\operatorname{div} \mathbf{V} = 0 \tag{1}$$

$$\frac{\partial \mathbf{V}}{\partial t} + (\mathbf{V}\cdot\operatorname{grad})\mathbf{V} = -\operatorname{grad} p + Re^{-1}\Delta\mathbf{V} + Ri\,T\mathbf{e} \tag{2}$$

$$\frac{\partial T}{\partial t} + (\mathbf{V}\cdot\operatorname{grad})T = (Re\cdot Pr)^{-1}\Delta T \tag{3}$$

in which, $\mathbf{V} = (u, v, w)$ is the velocity, p the pressure, T the temperature, $\mathbf{e} = (0, 1, 0)$ the unit vector in the vertical direction. The reference scales for nondimensionalization are h, U_0, h/U_0 and ρU_0^2 for length, velocity, time and pressure, respectively. The nondimensional temperature T is defined as $(T_{\text{dim}} - T_B)/\Delta T$. The relevant nondimensional parameters are the Reynolds number $Re \equiv U_0 h/\nu$; the Grashof number $Gr \equiv \alpha g \Delta T h^3/\nu^2$, in which α denotes the coefficient of thermometric expansion of the fluid, and g gravity; Prandtl number $Pr = \nu/\kappa$; and the mixed-convection parameter $Ri \equiv Gr \cdot Re^{-2}$.

The boundary conditions are

$$\mathbf{V} = (1,0,0) \quad \text{at} \quad y = 1$$

$$\mathbf{V} = 0 \quad \text{at} \quad y = 0, \quad x = 0,1 \quad \text{and} \quad z = 0,1$$

$$T = 0 \quad \text{at} \quad y = 0$$

$$T = 1 \quad \text{at} \quad y = 1.$$

$$\frac{\partial T}{\partial n} = 0 \quad \text{at} \quad x = 0,1 \quad \text{and} \quad z = 0,1$$

where n denotes the normal direction to the surface.

The initial conditions are such that the fluid is motionless and the vertically linear temperature profile is prescribed.

The above system of equations is solved by using the MAC (Marker and Cell) method. The Poisson equation, which is derived by taking the divergence of the momentum equations, is solved iteratively by utilizing the SOR (Successive Over-Relaxation) technique. The pressure field is introduced into the momentum equations to calculate the velocity field at the next time level. An explicit time-stepping is used in the momentum and energy equations.

The accuracy of discretizations is second-order in space and first-order in time. The grid points are clustered near the solid boundary walls by employing hyperbolic tangent functions. The details of numerical procedures were given in previous accounts [e.g. 14, 17].

For the present three-dimensional calculations, the number of grid points was typically $(81 \times 81 \times 81)$. The time interval Δt was set 0.002 when $Ri \leqslant 1$ and 0.001 when $Ri > 1$. Extensive sample runs were performed to ascertain the grid- and time-step convergences of the numerical output. The outcome of these elaborate sensitivity tests was highly positive, which established the reliability and accuracy of the present numerical methodologies. The CPU time was 10–20 h per run on an NEC SX3/21 supercomputer (maximum speed 1.6×2 GFLOPS, main memory 256M bytes).

3. RESULTS AND DISCUSSION

The present results indicate that solutions are not steady when Re exceeds approximately 2000. The principal aim here is to address the character of flow when steady, converged solutions are secured and, for this reason, discussions will be concentrated on steady flows for three sets of Re = 100,400 and 1000. The Prandtl number is set at $Pr = 0.71$. The values of Gr are chosen such that the mixed-convection parameter Ri takes 0.001, 1.0 and 10. These three cases signify respectively the situations in which the buoyancy-driven stabilizing effect is vanishingly small, comparable to, and dominant compared to the influence of mechanically driven forced convection.

The objective is to illuminate the effects of the mechanically driven lid motion and of the thermally driven buoyancy on the global three-dimensional flow field. The numerical results are post-processed to exhibit: (A) the primary flows (u, v) on the $(x$–$y)$ plane at $z = 0.5$, and (B) the meridional flow (v, w) on the $(y$–$z)$ plane at $x = 0.5$.

Figure 2 shows the flow, computed at $Re = 400$, which illustrates the influence of Ri. Frames (A) portray the $(u$–$v)$ velocity projections on the plane of z = const., and frames (B) the $(v$–$w)$ velocity projections on the plane of x = const. Since steady-state flows are considered, the path lines and the streamlines are identical. Three-dimensional perspective views, which may be obtained by combining frames (A) and (B), do not yield clear pictures, and Fig. 2 displays separate frames of (A) and (B). When the buoyancy effect is very small (see Fig. 2a), frame (A) depicts the well-documented (u, v)-velocity pattern of the benchmark solution. The main clockwise circulation cell fills much of the cavity interior, and a weak counter-clockwise cell is seen at the lower-right corner. This is typical of the primary flow in a mechanically-driven cavity of a non-stratified fluid when Re is reasonably high. The associated meridional (v, w)-flow has also been studied extensively. The pictures shown in Fig. 2a reproduce much of the eminent features of conventional driven-cavity flows.

As the strength of stable stratification increases, the major part of the primary clockwise circulation cell tends to be located in the upper region of the cavity closer to the top surface (see Fig. 2b). The stable stratification suppresses vertical motions, and, therefore, the impact of the sliding top wall penetrates to smaller distance into the fluid. As seen in Fig. 2(c), when Ri is large, the flow in the middle and lower portions of the cavity interior is meager. The weakening of vertical motions with the increase of Ri is also apparent in the meridional flows. Also, as stable

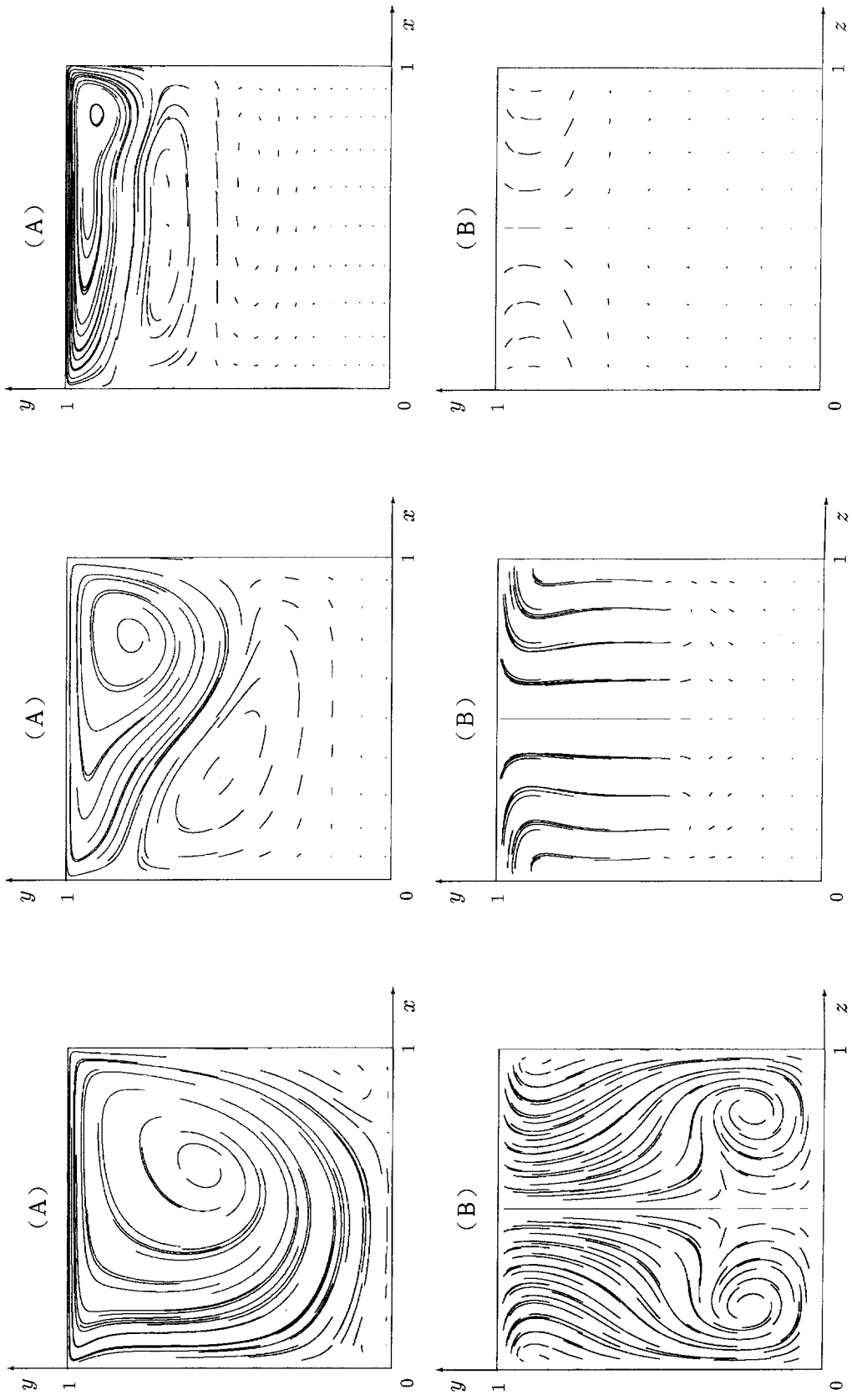

Fig. 2. Plots of: (A), $(u$–$v)$ velocities at $z = 0.5$; (B), $(v$–$w)$ velocities at $x = 0.5$. (a) $Ri = 0.001$, $Re = 400$; (b) $Ri = 1.0$, $Re = 400$; (c) $Ri = 10.0$, $Re = 400$.

stratification increases (see Fig. 2c), the principal part of meridional flows tends to be located to the upper region closer to the sliding wall. The illustrations in Fig. 2 serve to identify the major qualitative changes in the global flow patterns as Ri encompasses a wide range.

Figure 3 exhibits the overall flow characteristics as Re varies. Several attempts have been made to produce well-balanced three-dimensional descriptions. In Fig. 3, coordinates and scales have been adjusted to select suitable viewing angles of the cavity flow. Frames (A) illustrate the cases of a non-stratified fluid ($Ri = 0.001$). The intensification of three-dimensionalities, which are represented by distinct meridional flows and by the dependence of the flow on the z-coordinate, is discernible as Re increases. These aspects were elucidated in preceding reports regarding flows of a homogeneous fluid in a cubic driven-cavity [14, 15]. Frames (B) show the flows under substantial influence of stable buoyancy ($Ri = 10.0$). The suppression of vertical velocities, especially in the middle and bottom portions of the cavity, is notable, and this trend is more pronounced as Re increases. As manifested in frame (B) of Fig. 3(c), when $Ri \geqslant 1$ and Re is large, the fluid in the bulk of the cavity interior is nearly stagnant, except in a narrow region adjacent to the sliding top wall. The flows are mostly in the x-direction and they are localized to the top portion of the cavity interior. Extremely weak secondary flows are seen. In addition, in much of the interior, the dependence of the flow on the z-coordinate is minimal, pointing to the prevailing two-dimensionality. The meridional velocities when $Ri \geqslant 1$ and Re large are generally very small in the entire flow domain. The purpose of the work at this stage is to portray the global flow patterns in a realistic cavity. More precise descriptions of the three-dimensional flow details in the parameter space of Re and Ri are beyond the scope of the present endeavor.

The qualitative features of the thermal field are demonstrated by plotting the perspective views, as shown in Fig. 4. Frames (A) illustrate the iso-surfaces of temperature when Ri is negligibly small, indicating that the mechanically driven convection dominates the buoyancy-driven convection. When Re is reasonably small (see Fig. 4a for $Re = 100$), the iso-surfaces of temperature display a fair degree of two-dimensionality. As can be inferred by frame (A), temperature gradients are very small in a large interior portion surrounding the upper-right corner of the cavity. This is indicative of the existence of a region of intense mechanically driven convective activity, in which fluids are well mixed. When Ri is large, the stabilizing influence of buoyancy is dominant, and heat transfer is controlled mostly by conduction. Frame (B) of Fig. 4a is consistent with this assertion. Three-dimensionalities are very weak when Ri is large.

The thermal field characteristics at higher values of Re are described in Fig. 4b and c. When Ri is very small and Re large [see frame (A) of Fig. 4c], three-dimensionalities of the thermal field are pronounced. The vertical temperature gradients are confined mostly to the boundary layer regions near the top and bottom horizontal walls. In the bulk of the interior, fluids are well mixed by virture of intensified mechanically driven convection.

However, in the opposite limit, when Ri is large, the convective activities are inhibited by stable stratification. The heat transport is predominantly conductive, and this trend becomes more pronounced as Re increases. The temperature field is strongly two-dimensional and isothermal surfaces are nearly horizontal, as exemplified in frame (B) of Fig. 4c.

Based on the temperature field data, the local Nusselt number Nu distributions on the top heated wall and bottom cooled wall are plotted in Fig. 5. When Ri is large[see frames (B) of Fig. 5], the Nu-values at the bottom wall are close to unity. This reflects the fact that, in the lower region of the cavity, fluid motions are suppressed and heat transfer is dominated by conduction. On the upper portion of the cavity, weak fluid motions are seen. Generally, the Nu-values are small, and the Nu-distributions are mostly two-dimensional in the left portion of the top wall. Slight three-dimensional features in Nu are seen in the right portion of the top right wall. These trends are more pronounced as Re increases. On the other hand, when Ri is very small, frames (A) of Fig. 5 illustrate the substantial impacts of forced convection. Especially when Re is large, the Nu-distributions at the walls exhibit complex behavior, both in the z-direction as well as in the x-direction. The Nu-values at the top wall are very large at the top-left corner of the container, and Nu tends to decrease as x increases. On the bottom wall, due to the presence of vigorous convective activities in the entire cavity, the Nu values peak in the middle portion. At both the top and bottom wall, three-dimensional variations in Nu are notable as Re increases.

In engineering applications, the overall effectiveness of heat transfer between two horizontal walls is of relevance. For this purpose, the average Nusselt number $\bar{N}u$ is defined:

$$\bar{N}u = \int_0^1 \int_0^1 \left.\frac{\partial T}{\partial y}\right|_{y=0,\text{or}1} \mathrm{d}x\,\mathrm{d}z. \tag{4}$$

Table 1 lists the $\bar{N}u$ values at the top wall for the computations rendered. Obviously, if the top wall is stationary, the only heat transfer mode will be conduction, and $\bar{N}u = 1.0$. The convective activities which are induced by the moving wall clearly enhance

Table 1. The average Nusselt number $\bar{N}u$ at the top wall

Re	$Ri = 0.001$	$Ri = 1.0$	$Ri = 10.0$
10^2	1.82	1.33	1.08
4×10^2	3.99	1.50	1.17
10^3	7.03	1.80	1.37

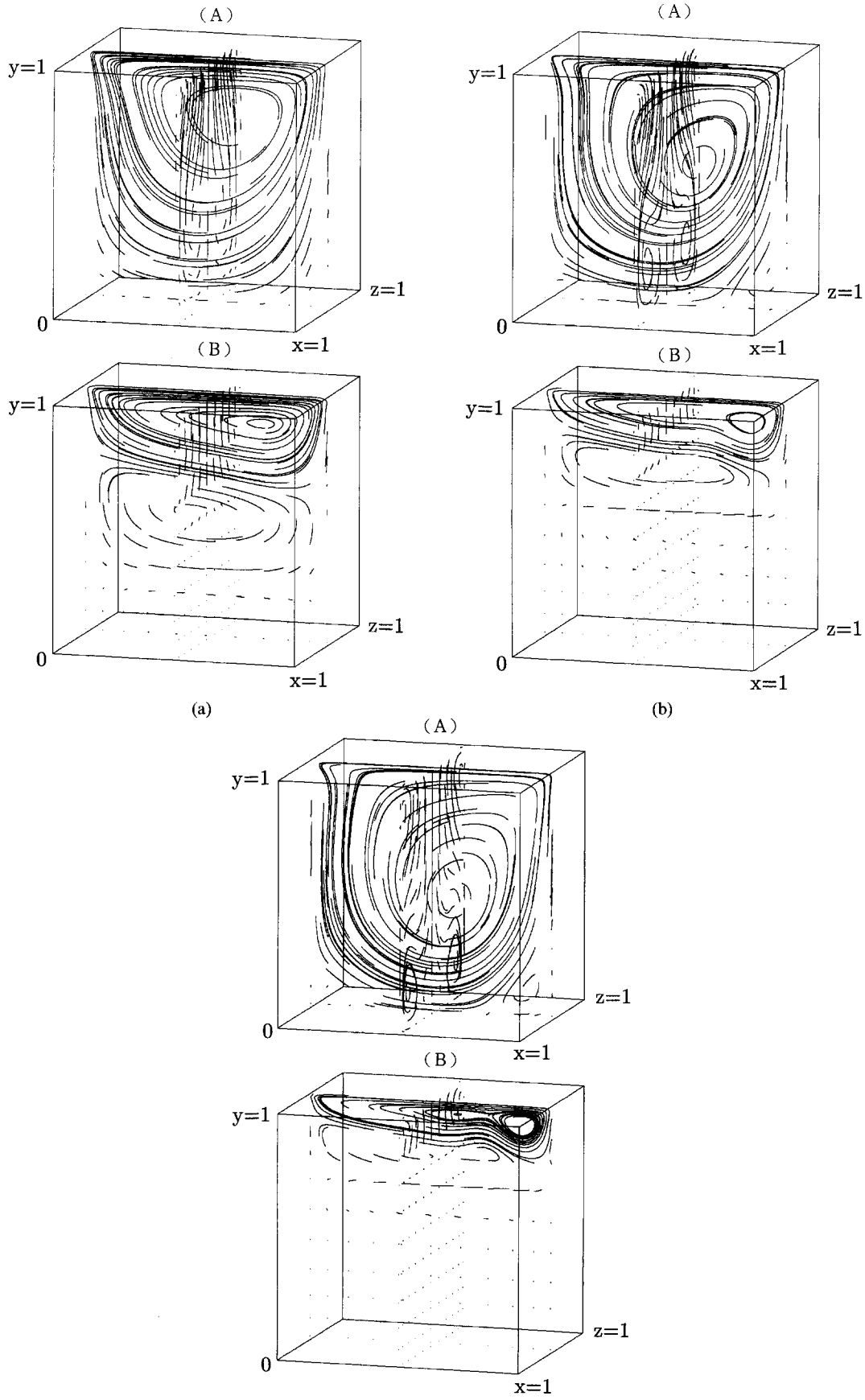

Fig. 3. Effects of Re on global flow field. Frames (A) show the results of very small Ri($Ri = 0.001$), and frames (B) for $Ri = 10.0$. (a) $Re = 100$; (b) $Re = 400$; (c) $Re = 1000$.

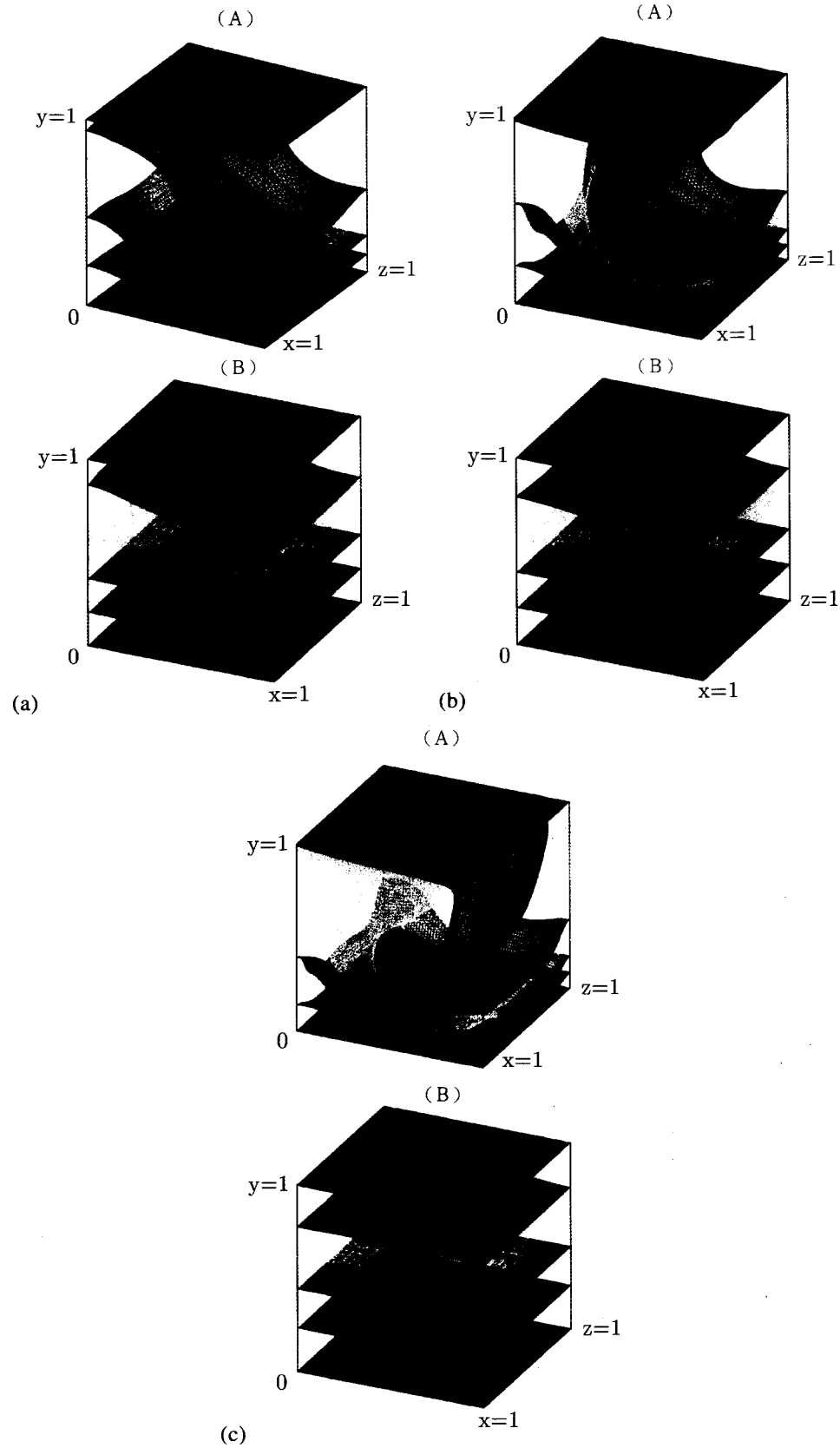

Fig. 4. Effects of *Re* on thermal fields. The contour values of isotherms are, from bottom to top, 0.0 (dark blue), 0.2 (light blue), 0.4 (green), 0.6 (yellow), 0.8 (bright red), 1.0 (dark red). Frames (A) are for $Ri = 0.001$, and frames (B) for $Ri = 10.0$. (a) $Re = 100$; (b) $Re = 400$; (c) $Re = 1000$.

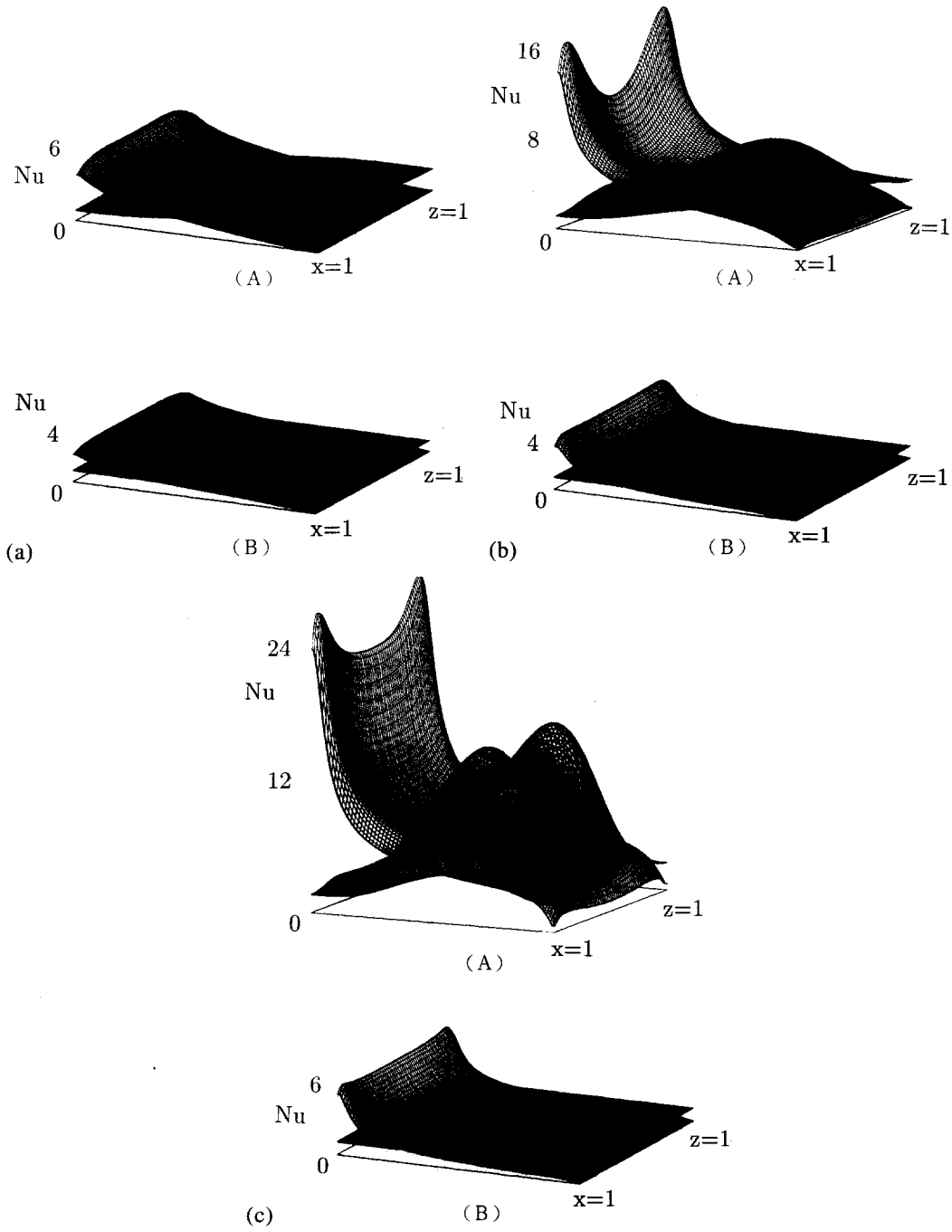

Fig. 5. The *Nu* distributions on the top heated wall (shown in red) and on the bottom cooled wall (blue). Frames (A) are for $Ri = 0.001$, and frames (B) for $Ri = 10.0$. Conditions are: (a) $Re = 100$; (b) $Re = 400$; (c) $Re = 1000$.

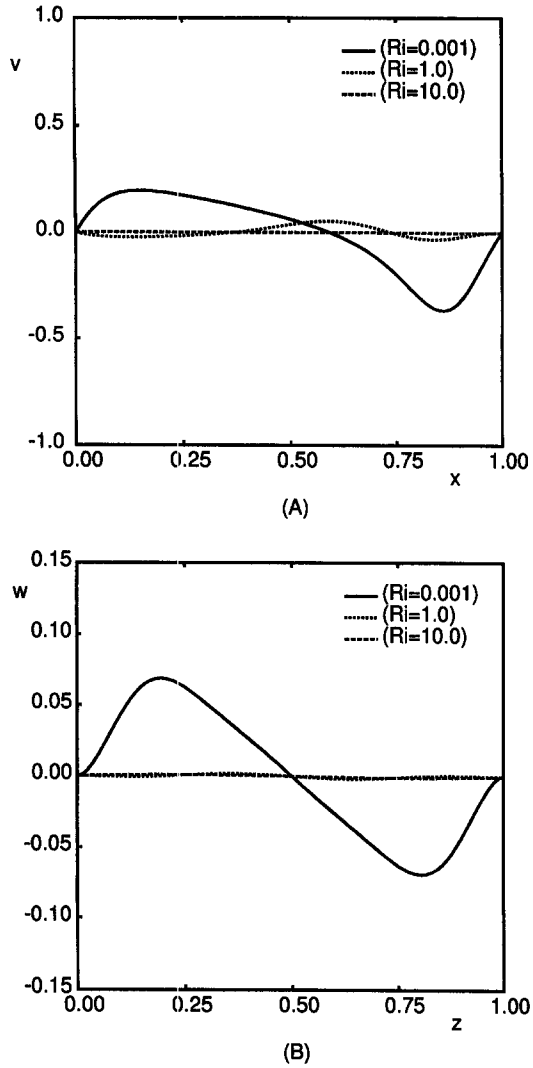

Fig. 6. Exemplary plots of the secondary flow profiles. (A) (v–x) plots at $y = 0.5$, $z = 0.5$. $Re = 400$, $Pr = 0.71$. (——) $Ri = 0.001$; (. . .) $Ri = 1.0$; (–) $Ri = 10.0$. (B) (w–y) plots at $x = 0.5$, $z = 0.5$. $Re = 400$, $Pr = 0.71$. (——) $Ri = 0.001$; (. . .) $Ri = 1.0$; (–) $Ri = 10.0$.

the overall heat transfer. The augmentation of heat transfer becomes more effective as Re increases and Ri decreases. Many of the computational results shown here are indicative of the qualitative effects of Re and Ri on the overall flow. Quantitative comparisons of the convective and buoyancy effects are also informative. As an example, Fig. 6 gives exemplary plots of secondary velocity profiles, which allow more detailed cross-comparisons of these two effects.

4. CONCLUSION

Comprehensive numerical computational results have been acquired for three-dimensional flows in a cubical cavity. Numerical flow visualizations demonstrate the explicit effects of Ri as well as Re.

When Ri is very small, the gross flow characteristics are akin to the conventional driven-cavity flows, as addressed by earlier studies by Iwatsu *et al.* [14, 15]. When Ri is appreciable, both the primary and meridional flows are confined to the upper region of the cavity. In much of the middle and lower portion of the cavity, fluids tend to be stagnant and heat transfer is mostly conductive. Three-dimensional features, as represented by meridional flows, are intensified as Re increases.

When Ri is small at low values of Re, the isotherm surfaces maintain a fair degree of two-dimensionality. When Ri is small and Re large, the thermal field shows stronger three-dimensionalities. On the other hand, stabilizing buoyancy effects become dominant at large Ri. In this case, heat transfer is largely convective and three-dimensionality in the thermal field is weak.

The influence of Ri is also apparent in the plots of Nu at the walls. When Ri is large, overall heat transport is suppressed, and the conductive heat transfer mode prevails. When Ri is very small, and especially when Re is large, complex three-dimensional features are discernible in the Nu-fields. The global heat transfer is enhanced by vigorous forced convection.

REFERENCES

1. M. Deville, T. H. Lê and Y. Morchoisne (eds), *Numerical Simulation of 3-D Incompressible Unsteady Viscous Laminar Flows, a GAMM-Workshop*, pp. 13–118. Vieweg, Wiesbaden (1992).
2. J. R. Koseff and R. L. Street, Visualization studies of a shear driven three-dimensional recirculation flow, *J. Fluids Engng* **106**, 21–29 (1984).
3. J. R. Koseff and R. L. Street, On end wall effects in a lid-driven cavity flow, *J. Fluids Engng* **106**, 385–389 (1984).
4. J. R. Koseff and R. L. Street, The lid-driven cavity flow: a synthesis of qualitative and quantitative observations, *J. Fluids Engng* **106**, 390–398 (1984).
5. O. Mochizuki, H. Yamabe and H. Yamada, Flow in a two-dimensional square cavity (a comparison between flow visualization experiment and numerical calculations), *Bull. JSME* **29** (258), 4103–4106 (1986).
6. A. K. Prasad, C. Y. Perng and J. R. Koseff, Some observations on the influence of longitudinal vortices in a lid-driven cavity flow, AIAA paper AIAA-88-3654-CP (unpublished) (1988).
7. A. K. Prasad and J. R. Koseff, Reynolds number and end-wall effects on a lid-driven cavity flow, *Phys. Fluids A* **1**(2), 208–218 (1989).
8. O. Mochizuki and M. Kiya, Three-dimensional vortical structure in a lid-driven square cavity, *Proc. Int. Con. Fluid Mechanics*, Chen-gdu, China (1991).
9. C. K. Aidun, N. G. Triantafillopoulos and J. D. Benson, Global stability of a lid-driven cavity with throughflow: flow visualization studies, *Phys. Fluids A* **3**(9), 2081–2091 (1991).
10. C. J. Freitas, R. L. Street, A. N. Findikakis and J. R. Koseff, Numerical simulation of three-dimensional flow in a cavity, *Int. J. Numer. Meth. Fluids* **5**, 561–575 (1985).
11. C. J. Freitas and R. L. Street, Non-linear transport phenomena in a complex recirculating flow: a numerical investigation, *Int. J. Numer. Meth. Fluids* **8**, 769–802 (1988).
12. H. C. Ku, R. S. Hirsh and T. D. Taylor, A pseudospectral method for solution of the three-dimensional

incompressible Navier–Stokes equations, *J. Comput. Phys.* **70,** 439–462 (1987).
13. C. Y. Perng and R. L. Street, Three-dimensional unsteady flow simulations: alternative strategies for a volume-averaged calculation, *Int. J. Numer. Meth. Fluids* **9,** 341–362 (1989).
14. R. Iwatsu, K. Ishii, T. Kawamura, K. Kuwahara and J. M. Hyun, Numerical simulation of three-dimensional flow structure in a driven-cavity, *Fluid Dyn. Res.* **5,** 173–189 (1989).
15. R. Iwatsu, J. M. Hyun and K. Kuwahara, Analyses of three-dimensional flow calculations in a driven cavity, *Fluid Dyn. Res.* **6,** 91–102 (1990).
16. R. Iwatsu, J. M. Hyun and K. Kuwahara, Driven cavity flow with stabilizing temperature stratification, AIAA paper AIAA-92-0713 (unpublished) (1992).
17. R. Iwatsu, J. M. Hyun and K. Kuwahara, Mixed convection in a driven cavity with a stable verical temperature gradient, *Int. J. Heat Mass Transfer* **36**(6), 1601–1608 (1993).
18. A. A. Mohamad and R. Vistanka, Combined surface shear and buoyancy-driven convection in a shallow cavity, *Proc. AIAA/ASME Thermophysics and Heat Transfer Conf.*, Seattle, WA (1990).
19. S. K. Sinha and S. Sengupta, An investigation of destratification in enclosed basins due to surface shear, *Proc. Winter Annual Meeting of The American Society of Mechanical Engineers*, Anaheim, CA (1986).